Inorganic Chemistry

Article

pubs.acs.org/IC

Reduced and Oxidized Forms of the Pt-Organometallic Version of Polyaniline

Tommy Kenny, Simon Lamare, Shawkat M. Aly,[†] Daniel Fortin,* Gessie Brisard, and Pierre D. Harvey*

Département de Chimie, Université de Sherbrooke, Sherbrooke, Quebec J1K 2R, Canada

Supporting Information

ABSTRACT: This work represents an effort to synthesize all four forms of polyaniline (PANI) in its organometallic versions. Polymers containing substituted 1,4-benzoquinone diimine or 1,4-diaminobenzene units in the backbone exhibiting the general structure $(C{\equiv}CC_6H_4{-}N{=}C_6X_4{=}N{-}C_6H_4C{\equiv}C\text{-}PtL_2)_n$ and $(C{\equiv}CC_6H_4NH\text{-}C_6X_4\text{-}NHC_6H_4C{\equiv}C\text{-}PtL_2)_n$ along with the corresponding model compounds $(C{\equiv}CC_6H_4{-}N{=}C_6X_4{=}N{-}C_6H_4C{\equiv}C)\text{-}(PtL_2Cl)_2$ and $(C{\equiv}CC_6H_4NH\text{-}C_6X_4\text{-}NHC_6H_4C{\equiv}C)\text{-}(PtL_2Cl)_2$ (L = PBu_3; X = H, F, Cl) were synthesized. The polymers and corresponding model compounds were characterized (including ^1H and ^{31}P NMR, IR, mass spectra, elemental analysis, and X-ray structure determinations) and investigated for their redox properties in the absence and in the presence of acid. Their optical properties, including ns transient spectroscopy were also investigated. These properties were interpreted through density functional theory (DFT) and time-dependent DFT (TDDFT) computations. These materials are found to be oligomers (GPC) with thermal stability (TGA) reaching 350 °C. The greatest stabilities were found in the cases with X = F. Using a data bank of 8 X-ray structures of diimine derivatives, a relationship between the C=N bond distance and the dihedral angle between the benzoquinone ring and the flanking phenyl planes is noted. As the size of the substituent X on the benzoquinone center increases, the degree of conjugation decreases as demonstrated by the C=N bond length. The largest dihedral angles are noted for X = Cl. These polymers exhibit drastic chemical differences when X is varied (X = H, F, Cl). The completely reduced polymer $(C{\equiv}CC_6H_4NH\text{-}C_6H_4{-}NHC_6H_4C{\equiv}C\text{-}PtL_2)_n$ (i.e., X = H) was not chemically accessible whereas in the cases of X = F, Cl, these materials were obtained and represent the first examples of fully reduced organometallic versions of PANI (i.e., leucoemaraldine). For the $(C{\equiv}CC_6H_4{-}N{=}C_6X_4{=}N{-}C_6H_4C{\equiv}C\text{-}PtL_2)_n$ polymers, the completely oxidized form for X = H was isolated (pernigraniline), but for X = F and Cl, only the largely reduced mixed-valence form (i.e., emaraldine) was obtained via chemical routes. In acidic solutions, the chemically accessible polymer for X = H, $(C{\equiv}CC_6H_4{-}N{=}C_6H_4{=}N{-}C_6H_4C{\equiv}C\text{-}PtL_2)_n$, exhibits two chemically reversible waves indicating that the reduced form $(C{\equiv}CC_6H_4NH\text{-}C_6H_4{-}NHC_6H_4C{\equiv}C\text{-}PtL_2)_n$ can be generated. The absorption spectra of the highly colored diimine-containing species exhibit a broad charge transfer band (assigned based on DFT calculations (B3LYP); $C_6H_4C{\equiv}C\text{-}PtL_2\text{-}C{\equiv}CC_6H_4 \rightarrow N{=}C_6X_4{=}N$) in the 450−800 nm window red shifting according X = H → Cl → F, consistent with their relative inductive effect. The largest absorptivity is measured for X = H because this polymer is fully oxidized whereas for the cases where X = F and Cl, these polymers exists in the mixed valence form. The ns transient absorption spectra of two polymers (X = F; reduced and mixed-valence polymers) were measured. The triplet excited state in the mixed-valence polymer is dominated by the reduced diamine residue and the $T_1\text{-}T_n$ absorption of the diimine is entirely quenched.

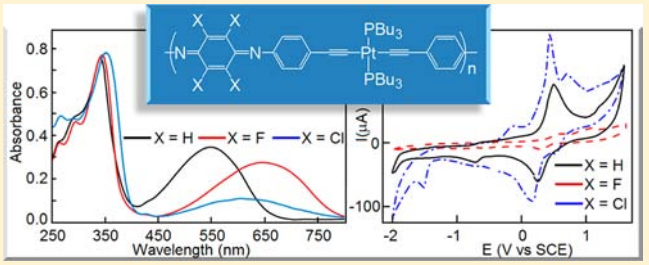

INTRODUCTION

Polyaniline (PANI) has been known for at least 150 years,[1] and is an important conducting and semiconducting polymer with numerous interesting properties and applications such as magnetism, biosensors, electronic noses, electrorheology, corrosion inhibitors, biocompatibility, organic coating, electrostatic dissipation or shielding, light emitting polymer devices, rechargeable batteries, fuel cells,[2] and more recently photocells.[2k−x] The various forms of PANI include the pernigraniline (oxidized form, insulator), leucoemaraldine (reduced form, insulator), emaraldine (mixed-valence, insulator), and protonated emaraldine form (electric conductor), Chart 1, in which the two easily recognizable submotifs are the *trans*-quinone diimine (see Chart 2) and the *para*-diaminobenzene.

Molecules and polymers containing the quinone diimine residue can provide materials with applications being as wide as corrosion prevention[3] and light emitting diodes (LED).[4] In such materials, the spectral signature in the UV−vis spectra is characterized by a low energy charge transfer (CT) band, which is also consistent of strong CT complexes between a donor and acceptor.[5] The chemistry and electrochemistry is intimately

Received: April 17, 2012
Published: November 21, 2012

Chart 1

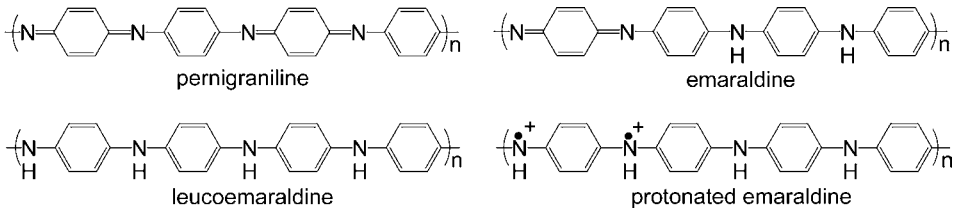

Chart 2

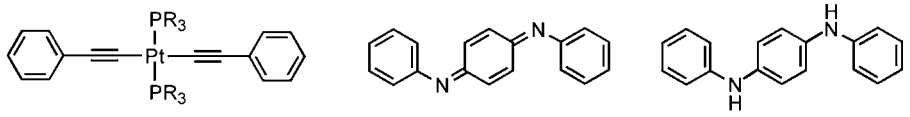

Chart 3

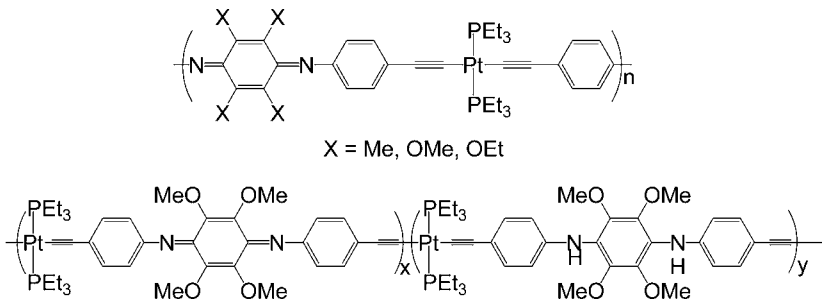

Chart 4

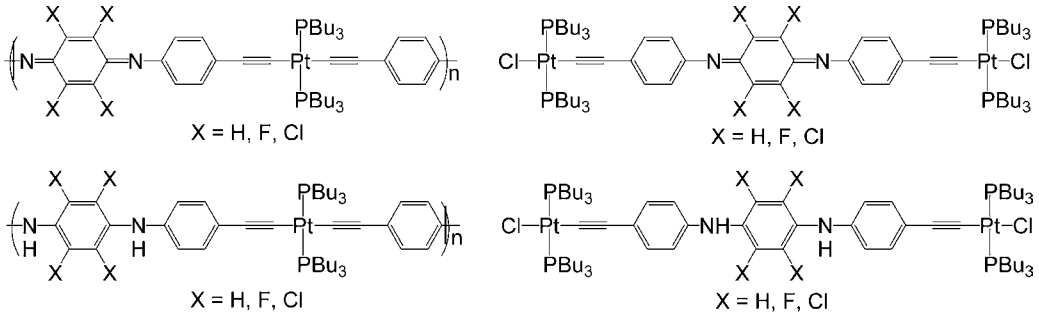

linked by the presence of a quinone diimine/diaminobenzene equilibrium.[6]

Conjugated $(A\text{-}B)_n$-type polymers built upon the quinone diimine unit and the *trans*-bis(ethynyl)bis(phosphine)platinum-(II) conjugated fragment (Chart 2) represent an organometallic version of PANI under its fully oxidized pernigraniline form or mixed-valence form (emaraldine) and have recently been the subject of investigations (Chart 3).[7]

The main conclusions are that these alternated polymers are electroactive in solution, luminescent in both frozen solution and the solid state at 77 K, and their physical properties are dependent on the dihedral angle between the average planes of the quinone diimine residue and the benzene rings often induced by steric interactions. So far, the investigated quinone diimine-containing organometallic polymers were strictly limited to methoxy and methyl substituents on the benzoquinone ring. Because of the low-lying CT excited state for the polymers and the fact that duroquinone (dichlorodicyanobenzoquinone; DDQ) a related compound that has a strong oxidizing ability, it became clear that more derivatives needed to be explored. For instance, what is the effect of using strongly electron withdrawing substituents such as fluorine, on the redox and CT properties of the polymeric materials? On the basis of previous findings, the CT process from the Pt-containing unit to the quinone diimine should be favored, and this low-energy band should be red-shifted as the substituents become more electron withdrawing. Furthermore, attempts also were made to prepare the fully reduced form (organometallic leucoemaraldine version) of these polymers but only the mixed valence form (emaraldine version) with methoxy substituents were employed.[7a] Similarly, unsuccessful attempts to prepare the reduced form for the tetramethyl derivative were made.

We now report the preparation and characterization of two series of conjugated organometallic polymers. They contain the substituted 1,4-quinone diimines or *para*-diaminobenzenes in the backbone of the polymer chain exhibiting the general structure $(-N{=}C_6X_4{=}N{-}C_6H_4C{\equiv}C\text{-}PtL_2\text{-}C{\equiv}CC_6H_4\text{-})_n$ and $(-NH\text{-}C_6X_4\text{-}NH\text{-}C_6H_4C{\equiv}C\text{-}PtL_2\text{-}C{\equiv}CC_6H_4\text{-})_n$ along with the corresponding model compounds $(C{\equiv}CC_6H_4{-}N{=}$

dx.doi.org/10.1021/ic300775n | Inorg. Chem. 2012, 51, 13081−13095

Scheme 1[a]

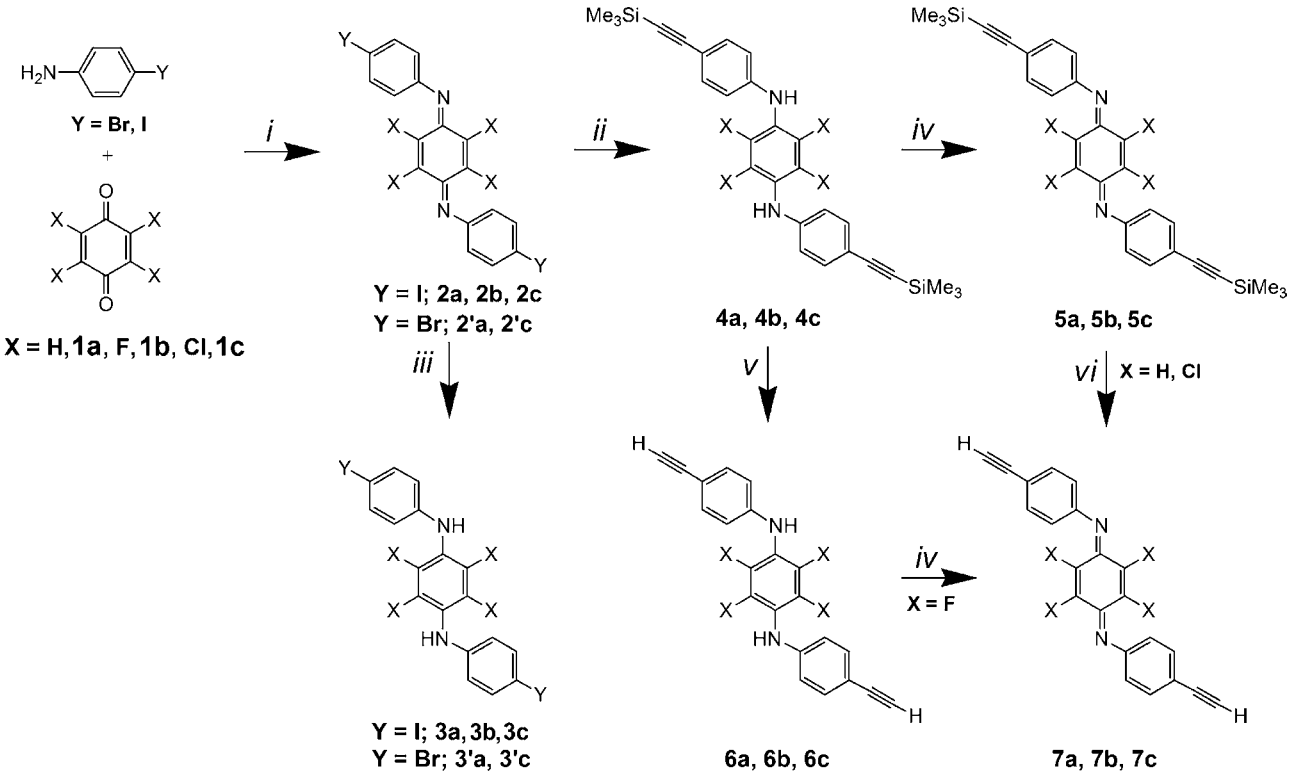

[a](*i*) $TiCl_4$, 1,4-diazabicyclo[2.2.2]octane, PhCl, 120 °C, 12 h for **2a** and **2′a**, 60 °C, 10 h for **2c** and **2′c**, 60 °C, 5 h for **2b**; (*ii*) $Me_3Si{-}C{\equiv}CH$, $PdCl_2(PPh_3)_2$, PPh_3, CuI, $^iPr_2NH$, PhMe, 60 °C, 12 h; (*iii*) $NaBH_4$ EtOH(abs), CH_2Cl_2,60 min; (*iv*) ∼10 equiv of 2,3-dichloro-5,6-dicyano-1,4-benzoquinone, CH_2Cl_2 for **5a** and **5c**, $CHCl_3$, ∼4 equiv of 2,3-dichloro-5,6-dicyano-1,4-benzoquinone, 20 min, RT for **7b**; (*v*) ∼5 equiv of 0.1 M NaOH/H_2O, THF, RT for **6b**, K_2CO_3, CH_3OH, 6 h for **6a** and **6c**. (*vi*) CH_2Cl_2, TBAF, 4 h for **7a** and **7c**. Note that **3b** was obtained as a side product while forming **2b**.

$C_6X_4{=}N{-}C_6H_4C{\equiv}C)(PtL_2Cl)_2$ and $(C{\equiv}CC_6H_4{-}NH\text{-}C_6X_4\text{-}NH\text{-}C_6H_4C{\equiv}C)(PtL_2Cl)_2$ where L = PBu_3, X = H, F, Cl, (Chart 4). The optical and electronic properties are investigated in detail, which are accompanied by DFT (Density Functional Theory) and TDDFT (Time-Dependent DFT) computations.

EXPERIMENTAL SECTION

See the Supporting Information.

RESULTS AND DISCUSSION

Synthesis and Characterization. The synthesis of the benzoquinone and 1,4-diaminobenzene spacers proceeds using the commercially available tetra-substituted benzoquinones and using standard procedures (Scheme 1). It proceeds by a condensation of benzoquinones (X = H, F, Cl) with 2 equiv of substituted p-aniline (Y = Br, I) in the presence of *fresh* $TiCl_4$ to produce the corresponding quinone diimines. The subsequent anchoring of the ethynyltri-methylsilane residue proceeds in Sonogashira conditions with $[PdCl_2(PPh_3)_2]$ and CuI but unexpectedly forms the corresponding reduced diaminobenzene analogues (**4a**, **4b**, **4c**), which can then be oxidized by DDQ to the desired oxidized products **5a** and **5c**. Compound **5b** (X = F) was prepared as previously reported from the direct reaction between tetrafluoroquinone and 4-[(trimethylsilyl)ethynyl]aniline in the presence of $TiCl_4$.[7c] The deprotection of compounds **4a**, **4b**, **4c** leads to the reduced spacers **6a**, **6b**, **6c**. The latter compound **6b** can then be oxidized by DDQ to afford the desired oxidized spacer **7b**, without substitution of the fluorides. Finally, **5a** and **5c** can be deprotected in the usual manner with TBAF to form **7a** and **7c.** The key characterization features are the confirmed presence or absence of ν(C═N), ν(C≡C), and ν(N−H) and δ(NH) in the IR and ^{1}H NMR spectra, respectively ($1620 < \nu(C{=}N) < 1635$; $2139 < \nu(C{\equiv}CSiMe_3) < 2157$ and $2093 < \nu(C{\equiv}CH) < 2104$; $3400 < \nu(N{-}H) < 3420$ cm^{-1}; $5.40 < \delta(NH) < 5.60$ ppm), and X-ray structure determination (Figure 1).

During the course of this study, four dihalogenated bis(*para*-benzene)-1,4-diaminobenzene building blocks were prepared (**3a**, **3c**, **3′a**, **3′b**). Compound **3b** was isolated as a side product during the synthesis of **2b**. The purpose was to construct a data bank of X-ray structures for a better characterization of the investigated spacers (**6a**, **6b**, **6c**, **7a**, **7b**, and **7c**) besides preparing synthons that can easily be modified (via Sonogashira reactions for example). The X-ray structures are presented in Figure 1, and the key data are summarized in Tables 1 and 2. These data are complemented with 2 cases where X = Me (**3d** (unpublished) and **5d** from reference 7b; Chart 5).

There is a clear correlation between the average dihedral angle between the average benzoquinone plane and that of the phenyl groups and the nature of the substituent X. Indeed, the van der Waals radii for H, F, and Cl are 1.30, 1.35, and 1.80 Å, and the average dihedral angles are 56.2, 52.2, and 75.2°, respectively. Similarly, in the reduced form, the *p*-diamino-benzene analogues, the equivalent average dihedral angles are 59.7 (X = H), 56.9 (X = F), and 73.5 (X = Cl). This comparison was also extended to X = Me assuming that its steric hindrance resembles that of X = Cl (Tables 1 and 2) and

dx.doi.org/10.1021/ic300775n | *Inorg. Chem.* 2012, 51, 13081−13095

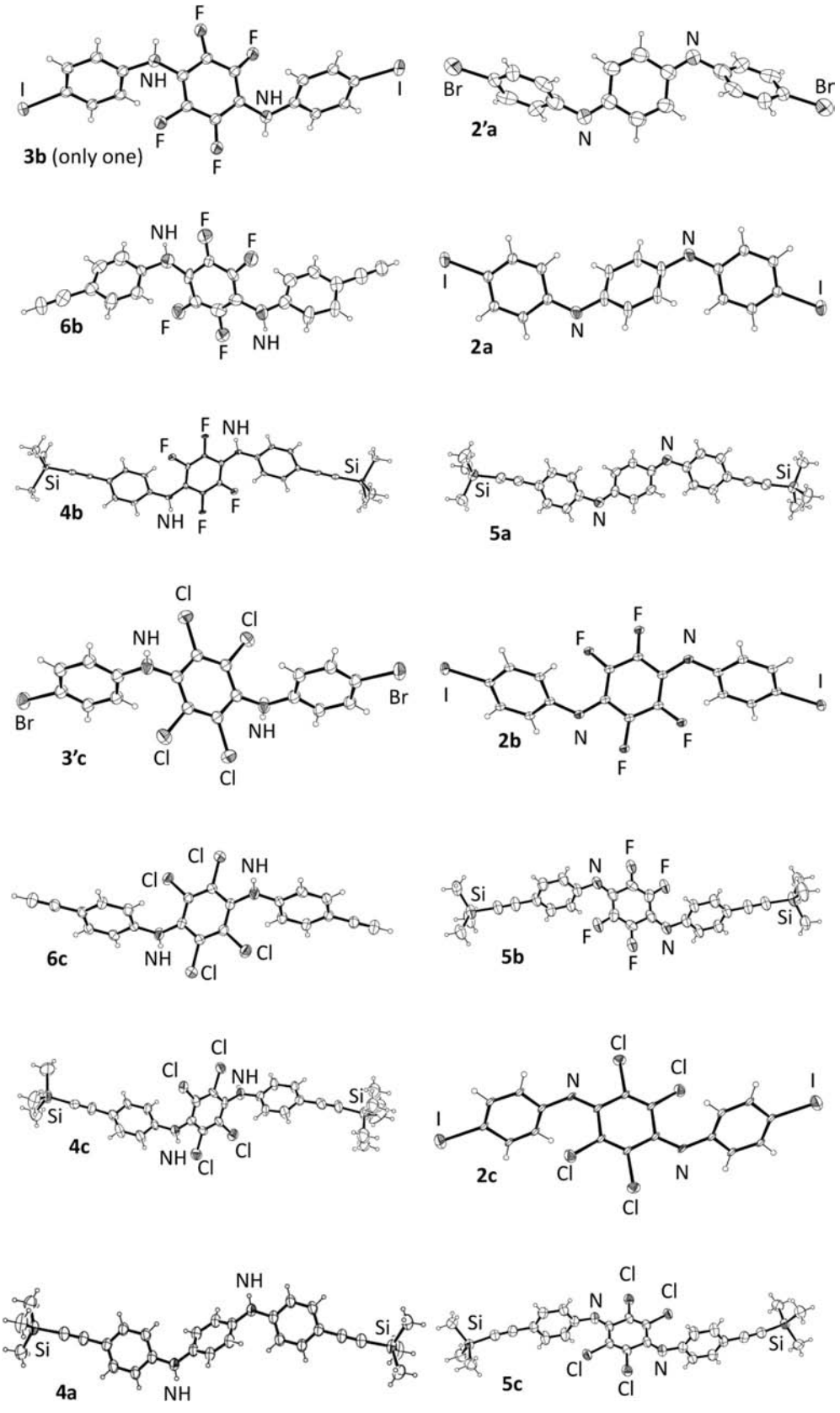

Figure 1. ORTEP representations of the investigated spacers. The thermal ellipsoids are represented at 30% probability.

indeed, the Me data compare more favorably to that of Br. This trend and the similarity in dihedral angle for same X-substituents strongly suggest that the degree of conjugation should be driven by steric effect in the quinone diimine spacers. Figure 2 exhibits this trend (broken gray line with ■ data points) where short C═N bond (weakly conjugated) are

dx.doi.org/10.1021/ic300775n | *Inorg. Chem.* 2012, 51, 13081−13095

Table 1. X-ray Average C═N Bond Distances and Dihedral Angles between the Average Benzoquinone Diimine Plane and That for the Phenyl Groups[a]

code	X	Y	d(C═N)/Å (esd)	dihedral angle/deg (esd)	average (deg)
2′a	H	Br	1.275 (0.036)	61.0 (3.8)	
2a	H	I	1.404 (0.054)	50.8 (5.1)	56.2 (X = H)
5a	H	C≡C -$SiMe_3$	1.309 (0.018)	56.9 (2.1)	
2b	F	I	1.339 (0.048)	49.7 (13.5)	52.2 (X = F)
5b	F	C≡C -$SiMe_3$	1.296 (0.027)	54.8 (2.6)	
2c	Cl	I	1.296 (0.040)	62.4 (9.0)	75.2 (X = Cl)
5c	Cl	C≡C -$SiMe_3$	1.261 (0.018)	88.1 (2.3)	
5d	Me	C≡C -$SiMe_3$	1.289 (0.012)	49.3 (0.9)	49.3 (X = Me)

[a]The crystal structures of **5b** and **5d** were reported previously (references 7c and 7b, respectively).

Table 2. X-ray Average *para*-C-N Bond Distances of the Central Benzene Ring and Dihedral Angles between the Average Benzene Ring Plane and That for the Phenyl Groups[a]

code	X	Y	d(C–N)/Å (esd)	dihedral angle/deg (esd)	average (deg)
4a	H	C≡C -$SiMe_3$	1.433 (0.015)	59.7 (1.7)	59.7 (X = H)
3b	F	I	1.386 (0.030)	57.5 (3.0)	
3b	F	I	1.404 (0.030)	55.7 (3.0)	
6b	F	C≡C–H	1.440 (0.015)	56.5 (1.6)	56.9 (X = F)
4b	F	C≡C -$SiMe_3$	1.389 (0.042)	55.7 (1.9)	
9b	F	C≡C -PtL_2Cl	1.380 (0.051)	59.0 (4.2)	
3′c	Cl	Br	1.396 (0.030)	66.6 (3.0)	
6c	Cl	C≡C–H	1.405 (0.015)	69.1 (1.6)	
4c	Cl	C≡C -$SiMe_3$	1.397 (0.030)	77.8 (3.6)	73.5 (X = Cl)
9c	Cl	C≡C -PtL_2Cl	1.337 (0.051)	80.7 (5.4)	72.3 (X = Me)
3d	Me	I	1.416 (0.030)	72.3 (3.0)	

[a]Two crystal structures were determined for **3b**. The synthesis, characterization and crystal structure of **3d** will be reported elsewhere.

Chart 5

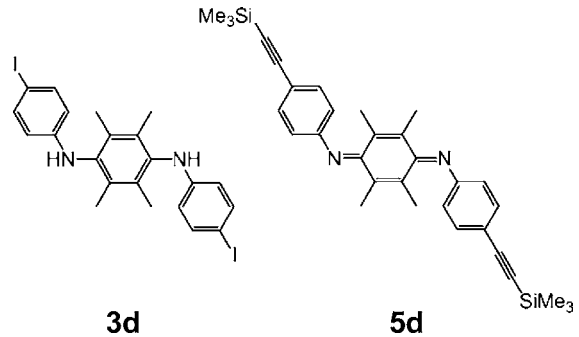

3d **5d**

associated with large dihedral angles, and vice versa. A systematic decrease (X = H, F, Cl) of the C═N bond length upon the replacement of the I-substituent at the *para*-positions of the phenyl groups by the conjugated group C≡C-$SiMe_3$ is observed.

The comparison of the C–N distances in the corresponding reduced and unconjugated *p*-diamino-benzene spacers as a function of the average dihedral angles between the average central benzene and phenyl planes exhibits a different trend. First, except for the Pt-containing model compounds **9b** and **9c**, the C–N bond length fluctuates between 1.39 and 1.44 Å. Second, the dihedral angle for X = F lies in a narrow window (57 ± 2°) and that for X = Cl lies in a longer (and larger) window (67–81°).

The synthesis of the model compounds **9b**, **9c**, **11a**, **11b**, and **11c** proceeds by reacting the corresponding spacers with an excess of *trans*-$PtCl_2(PBu_3)_2$ (Scheme 2). The remainder of the Pt-starting materials is recuperated. The synthesis of **9a** was not successful as it oxidized into **11a**. The reliable identification and characterization of the models is readily made from mass spectrometry, ^{31}P NMR where the coupling constant of Hz attests the *trans*-geometry about the Pt atom (2215 < $^1J(^{31}P–^{195}Pt)$ < 2514 Hz)[7b] and again the presence or absence of ν(C═N) and ν(N–H) and δ(NH) in the IR and ^{1}H NMR spectra, respectively (1620< ν(C═N) < 1635; 3400 < ν(N–H) < 3420 cm^{-1}; 5.40 < δ(NH) < 5.60 ppm) and the change in ν(C≡C) upon coordination of the Pt atom (2095 < ν(C≡C) < 2119 cm^{-1}). In two cases, X-ray structures were determined (Figure 3).

The crystal structures of **9b** and **9c** exhibit the expected dinuclear complexes where the square planar Pt atoms present the *trans*-geometry consistent with the characterization data (Figure 3). The bond distances and angles are normal (see selected data in the caption) for such Pt-complex and geometry. Interestingly, complexes **9b** and **9c** exhibit the shortest C–N bond lengths and the largest dihedral angles of their respective series (X = F and X = Cl, Me). π-back bonding may be responsible for this where the electronic density of the rich d^8 Pt(II) metal is pushed toward the electro-attractive group *p*-C_6F_4 and *p*-C_6Cl_4.

The fluctuating C–N bond length between 1.39 and 1.44 Å for the diaminobenzene spacers provides evidence of a single bond. The shorter 1.38 and 1.34 Å distances for X = F and Cl, respectively, suggest enhanced interactions with the central tetrasubstituted benzene. The key structural feature is the dihedral angle between the average benzene ring plane and that for the phenyl groups that places the dinuclear complexes at the larger end of Figure 2 in their respective series (X = F or Cl). Weak intramolecular steric hindrance could be invoked to explain this trend (especially when this angle is smaller for X = F), but the presence of two single bonds (C-NH-C) makes this angle difficult to interpret as crystal packing may influence this angle. An example for this is compound **3b** where two sets of crystal data were obtained (d(C–N) = 1.386 and 1.404 Å (esd =0.030 Å), dihedral angle = 57.50 and 55.74° esd = 0.30°, respectively).

The synthesis of the polymers proceeds in the same way as for the model compounds except that employed stoichiometry is rigorously 1:1 (Scheme 2). Polymer **8a** was not obtained because of instability. No attempt was made to find an alternative synthetic route. Again the reliable identification and characterization of the target polymers is readily made from GPC (Table 3), ^{31}P NMR where the coupling constant J confirms the *trans*-geometry about the Pt atom (2215 < $^1J(^{31}P–^{195}Pt)$ < 2514 Hz), again the expected change in ν(C≡C) upon coordination of the Pt atom (2095 < ν(C≡C) < 2120

dx.doi.org/10.1021/ic300775n | *Inorg. Chem.* 2012, 51, 13081–13095

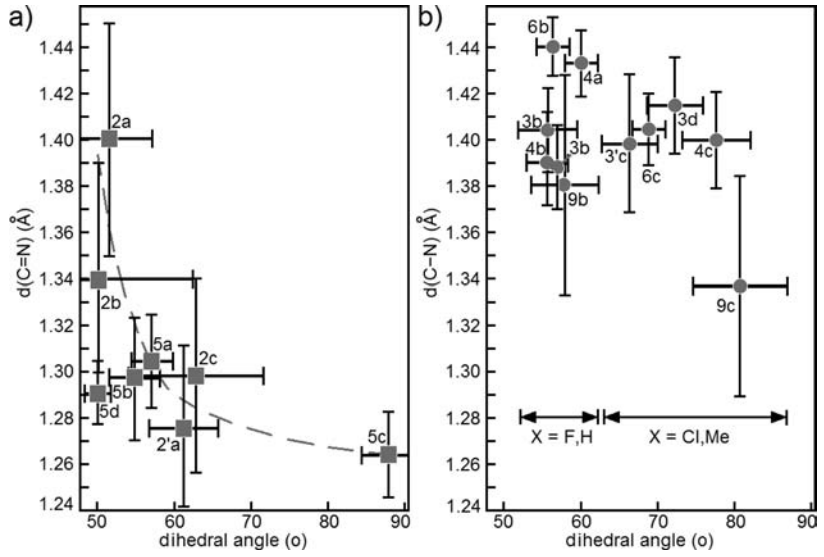

Figure 2. Comparison of the C═N distances in benzoquinone diimine spacers as a function of the average dihedral angles between the average quinone and phenyl planes (a) with the analogues (C–N) of the corresponding reduced *p*-diamino-benzene spacers (b). The bars are the esd's.

Scheme 2[a]

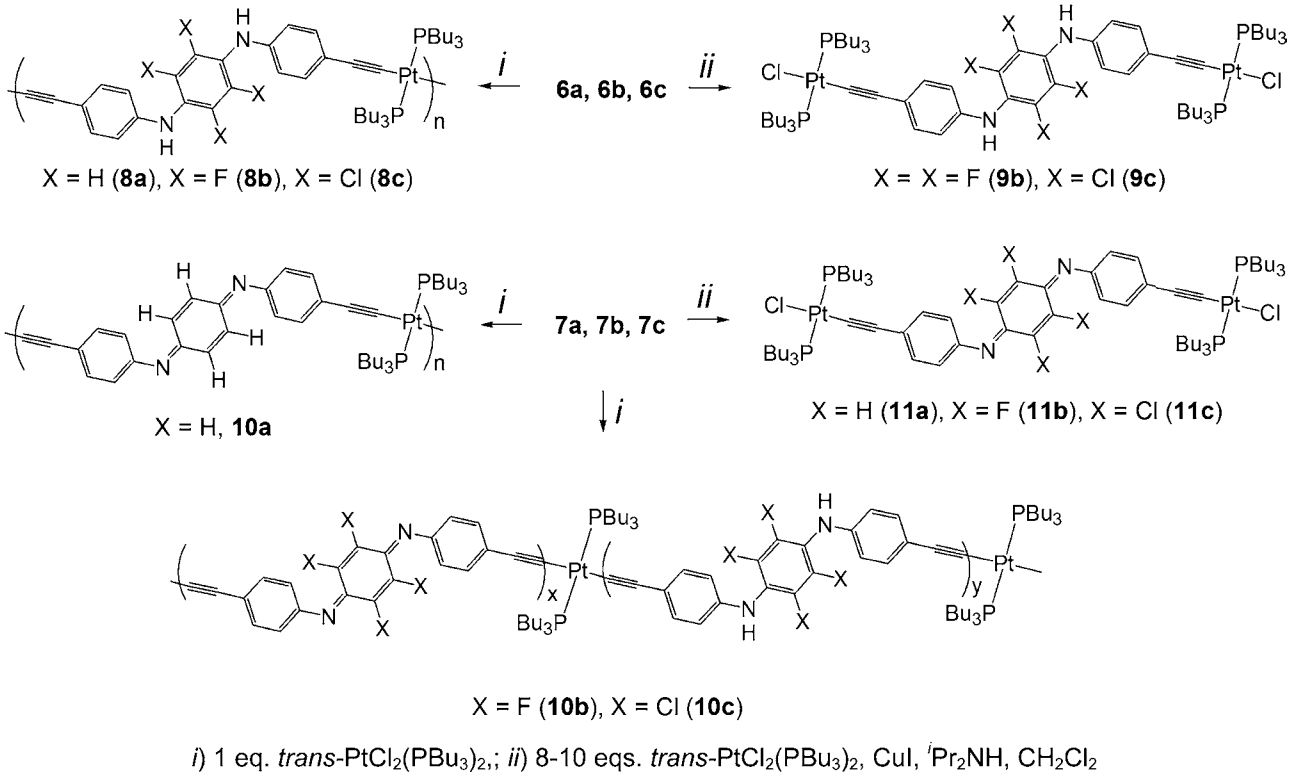

[a](*i*) 1 equiv of *trans*-$PtCl_2(PBu_3)_2$; (*ii*) 8–10 equiv of *trans*-$PtCl_2(PBu_3)_2$, CuI, $^iPr_2NH$, CH_2Cl_2

cm^{-1}), and the presence or absence of the characteristic signatures, ν(C═N) and ν(N–H), and δ(NH), in the IR and ^1H NMR spectra, respectively. Polymers **10b** and **10c** were obtained as mixed diimine/diamine materials as observed in the ^1H NMR and IR spectra. The relative amount of diamines in the polymers varies from sample to sample, and the electrochemical studies below demonstrated that the homopolymers could be generated from one another depending on the conditions in acid and applied potential.

The polymers were also characterized by GPC (Table 3). These materials are essentially oligomers, which is consistent for this family of polymers.[7] Similarly, the PDI values are high but are not unusual for the type of reaction used for the polymerization.[7] Interestingly, both M_n and the average number of units decrease as X is changed from H to F to Cl. In our previous report,[7c] a relationship was made between the relative steric hindrance and the chain length using all 4 possible combinations of *cis-trans* and *para-cis* isomers. In this work,

dx.doi.org/10.1021/ic300775n | *Inorg. Chem.* 2012, 51, 13081–13095

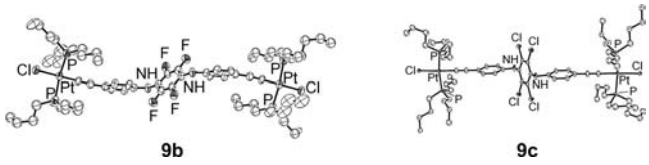

Figure 3. ORTEP representations of the model compounds **9b** and **9c**. The ellipsoids are shown at 30% thermal probability, and the H-atoms are not shown for clarity. Selected distances (Å) and angles (deg): **9b**; Pt−Cl: 2.339(4), Pt−P: 2.293(4), 2.297(4), Pt−C: 1.89(1), C≡C: 1.22(2), CPtCl: 179.3(5), PPtP: 171.8(2), ClPtP: 93.8(2), 94.0(2), CPtP: 86.7(5), 85.4(5). **9c**; Pt−Cl: 2.357(4), Pt−P: 2.292(4), 2.303(4), Pt−C: 2.035(8), C≡C: 1.143(9), ClPtC: 179.7(3), PPtP: 170.5(1), ClPtP: 95.2(2), 94.3(2), CPtP: 85.2(5), 85.5(5).

Table 3. GPC Data[a]

GPC	M_n	M_w	PDI
10a	24 700 (26.3)	44 800	1.81
8a[b]			
10b	14 600 (14.4)	38 000	2.61
8b	14 300 (14.2)	23 400	1.63
10c	11 700 (10.9)	22 300	1.97
8c	11 800 (10.9)	30 400	2.57

[a]The values in brackets are the average number of units. [b]Polymer not available.

steric hindrance can also be invoked but the nature of the halide may also play a role.

The TGA traces for **10a** and **8b** reveal stability up to 300 °C. The comparison between **10a** and **8b** indicates an increase of thermal stability for the F-containing materials (Figure 4).

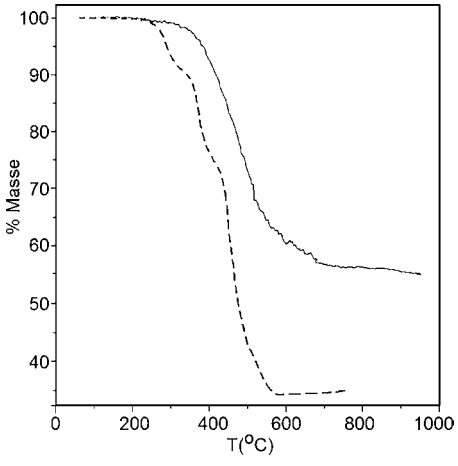

Figure 4. TGA traces of **10a** (dotted line) and **8b** (solid line).

Electrochemistry. The new materials were examined by cyclic voltammetry in the presence and the absence of acid (trifluoroacetic acid; TFA) to address the redox behavior of the spacers, model compounds and polymers. The cyclic voltammograms (CVs) of the diamine and the diimine species are presented in Figures 5 and 6, respectively. For most of the new materials characterized in this paper, the peak potentials resulting from both the anodic and the cathodic sweeps of the CVs are summarized in Table 4. It is known that *N,N′*-diphenylquinone diimine, which is a part of PANI, is electrochemically inactive in nonaqueous electrolytes,[8] and exhibits oxidation processes in its protonated form only.[9−11]

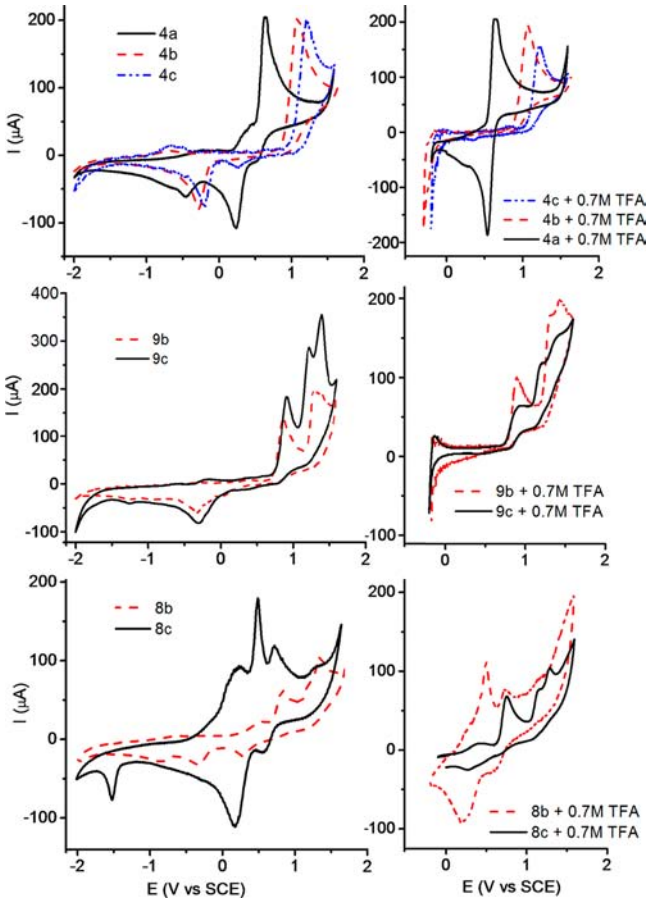

Figure 5. Top: Cyclic voltammograms (CVs) of the spacers **4a**, **4b**, and **4c** in the absence (left) and presence (right) of 0.7 M of TFA. Middle: CVs of the model complexes **9b** and **9c** in the absence (left) and presence (right) of 0.7 M of TFA. Bottom: CVs of the polymers **8b** and **8c** in the absence (left) and presence (right) of 0.7 M of TFA. All measurements were recorded against a saturated calomel electrode (SCE) with 0.1 M of $TBAPF_6$ supporting electrolyte in DMF. The concentration of the electroactive compounds was 4 mM. The scan rate is 100 mV/s. The scans were not exceeding −0.3 V when TFA was used because of strong H_2 evolution at more negative potentials.

The CVs of PhC≡CH exhibit an irreversible oxidation wave in the 1.5−2.0 V vs Ag/AgCl reference electrode.[12] This irreversibility is due to a radical-type polymerization process forming polyphenylacetylene.[12] The CV of *trans*- PhC≡CPt$(PBu_3)_2$C≡CPh was also studied in this work and compared well (SCE, this work, and Ag/AgCl reference electrodes have only 20 mV difference) with those of the literature.[13,14] This compound exhibits an irreversible oxidation peak at ∼1.2 V (weak) and 1.43 vs Ag/AgCl.[14] Some of the compounds could not be investigated because they decomposed in an acidic medium. This phenomena was reported before for other related species.[15] It is also interesting to note that an earlier work reported that the reduction wave of a related diimine compound is irreversible but becomes reversible upon coordination with a transition metal complex ion.[16]

The CVs reveal an electrochemically quasi-irreversibility behavior for all of the materials in absence of acid while the electrochemically irreversible process is enhanced in presence of acid. The positions of the peak potentials are scan rate dependent, which was verified for all cases. For comparison purposes the scan rate was set at 100 mV/s. In general, the CVs

dx.doi.org/10.1021/ic300775n | *Inorg. Chem.* 2012, 51, 13081−13095

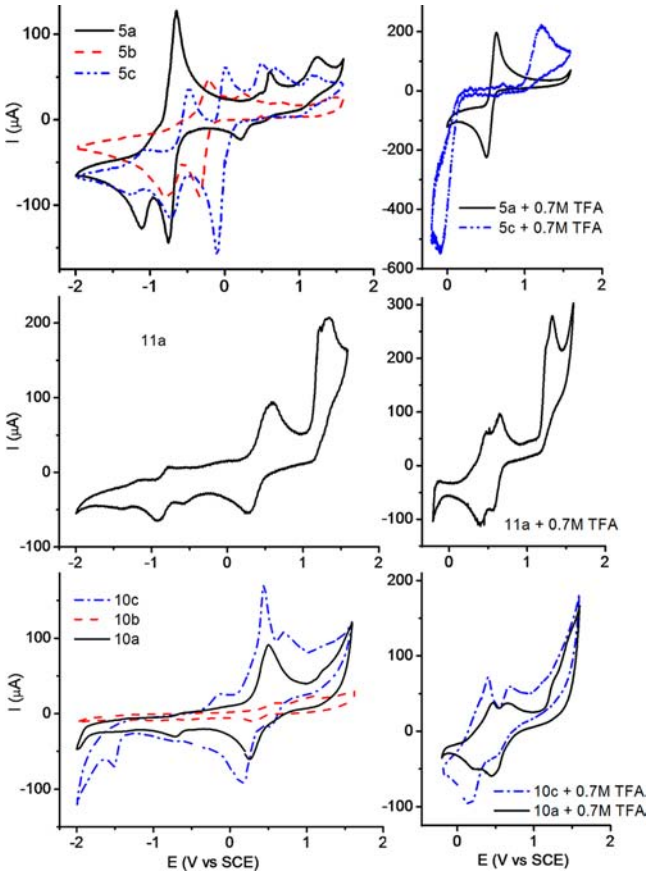

Figure 6. Top: Cyclic voltammograms (CVs) of the spacers **5a**, **5b**, and **5c** in the absence (left) and presence (right) of 0.7 M of TFA. Middle: CV of the model complex **11a** in the absence (left) and presence (right) of 0.7 M of TFA. Bottom: CVs of the polymers **10a**, **10b**, and **10c** in the absence (left) and presence (right) of 0.7 M of TFA. All measurements were recorded against a saturated calomel electrode (SCE) with 0.1 M of $TBAPF_6$ supporting electrolyte in DMF. The concentration of the electroactive compounds was 4 mM. The scan rate is 100 mV/s. The scans were not exceeding −0.3 V when TFA was used because of strong H_2 evolution more negative potentials.

Table 4. Cyclic Voltammograms Peak Potentials for the Anodic and Cathodic Sweeps[a]

	without TFA		with 0.7 M TFA	
	anodic sweep	cathodic sweep	anodic sweep	cathodic sweep
5a	−0.93[c], −0.65, 0.60, 1.20	0.22, −0.75, −1.08	0.63	0.51
5b	−0.22, 0.23w	−0.34, 0.78	dec.	dec.
5c	−1.06, −0.48, 0.01, 0.53, 0.69, 1.21	1.00, −0.1, −0.71, −1.25	1.22	−0.10
4a	0.40, 0.64	0.51, 0.24, −0.45	0.64	0.54
4b	1.09	−0.28	1.08	<−0.2
4c	−0.65w, 1.21	0.24, −0.21	1.22	0.34
11a	−1.17w, 0.78, 0.59, 1.23[c], 1.33	0.28, −0.57[b,c], −0.92, −1.42w	0.50, 0.65, 1.25, 1.32	0.55, 0.40
11b	*d*	*d*	*d*	*d*
11c	*d*	*d*	*d*	*d*
9a	*e*	*e*	*e*	*e*
9b	0.86, 1.32, 1.48[b]	−0.34, −1.27	0.90, 1.32, 1.43	<−0.2
9c	−0.16w, 0.91, 1.22, 1.39	−0.31, −1.27[b]	0.93, 1.21, 1.41	<−0.2
10a	0.51, 1.22	0.26, −0.71	0.46, 0.66, 1.27	0.46, 0.22
10b	0.61, 1.07	0.31, −0.95	dec.	dec.
10c	−0.13w, 0.44, 0.70, 1.23	0.52, 0.15, −1.52	0.41, 0.70	0.52, 0.15
8a	*e*	*e*	*e*	*e*
8b	0.50, 0.80, 1.16, 1.31	0.25, −0.36, −0.86	0.44, 0.80, 1.17, 1.33	0.34, < −0.2
8c	0.21, 0.46, 0.69, 1.24	0.52, 0.15, −1.52	0.50, 0.72, 1.18	0.57, 0.21
[**Pt**]	1.38	−0.32, −0.81w	1.38	−0.32, −0.81w

[a]Potentials reported vs SCE; in DMF; 0.1 M $TBAPF_6$; w = weak; dec = decomposition with acid. [**Pt**] = *trans*-$C_6H_5C{\equiv}C\text{-}PtL_2\text{-}C{\equiv}CC_6H_5$ (L = PBu_3). [b]Observed only during the first sweep, but not during the subsequent ones. [c]Weak and not well-defined beside a more intense signal. [d]Not measured. [e]Polymer not available, or decomposed in solution with acid.

for the diamine species are simpler than those for the corresponding diimines. This is due to the reduction processes of the diimine materials in the absence of H^+ ions that lead systematically to unstable species. The addition of H^+ ions does not influence much the shape of the CVs of the diamine species but leads to decomposition of some diimine species (such as **5b** and **10b**).

In some cases, the CVs clearly show the chemically reversible or quasi-reversible (not electrochemically reversible) behavior upon addition of H^+ ions. As an example, without TFA, the diamine compound **4a**, during the anodic sweep, is oxidized and releases H^+ ions at a given potential (Figure 5, top left). Upon the return sweep (i.e., cathodic sweep), these ions are diffused away from the anode and the cathodic wave is noted at 0.24 V. However upon addition of H^+ ions, the availability of these ions at the electrode vicinity is greater and consequently the wave for the cathodic reaction is recorded at a lesser cathodic potential (0.54 V). In the case of the corresponding diimine **5a**, the reduction predictably leads to unstable species which evolve during the scan. These newly generated reduced species exhibit their own electrochemical responses as weak irreversible waves in the oxidation region, as predicted. Upon addition of H^+ ions, the CV changes drastically and a new chemically reversible wave appears in the oxidation region of the CV. Importantly, this new wave is identical to that obtained in the case of **4a** meaning that the diamine and the diimine are clearly each other's products upon both oxidation and reduction, respectively, in the presence of H^+ ions. Under these conditions, these waves are considered quasi-reversible. However, this good correspondence between the diamine's and diimine's CV in the presence H^+ ions is not general. In some cases (see X = Cl; **5c** and **4c**, and **10c** and **8c**), the potential peaks are not rigorously identical. This may be related to a kinetic effect associated with the structural reorganization upon diamine-diimine conversion during the return sweep.

For one of the purposes of this work on polymers in acid solution, the chemically reversible or quasi-reversible waves were observed for **8b** (bottom red curve, Figure 5), **10a** and **10c** (bottom black and blue traces, respectively; Figure 6). The center of the cathodic and anodic sweeps are ∼0.40 and 0.60 for **10a**, 0.45 and 0.65 V vs SCE for **8b** and **10c**, reflecting the inductive effect. These polymer-acid systems represent the organometallic polymers in their protonated emaraldine forms.

The oxidation peak positions (Figure 5, top right) for the diamine spacers **4a**, **4b**, and **4c** (0.64, 1.08, 1.22 V vs SCE for X

dx.doi.org/10.1021/ic300775n | *Inorg. Chem.* 2012, 51, 13081−13095

= H, F, Cl, respectively) are again consistent with both the inductive effect (H vs F; similar dihedral angle; see discussion on the X-ray structures above), and the stabilization of the charge by conjugation (F is more stabilized because of the smaller dihedral angle in the diimine compounds vs Cl). This effect is also visible in the absence of H^+ ions (Figure 5 top left).

The interpretation of the redox behavior of the polymers can be performed by the comparison of the various fragments. For example, polymer **8b** (blue trace in Figure 7) can be analyzed

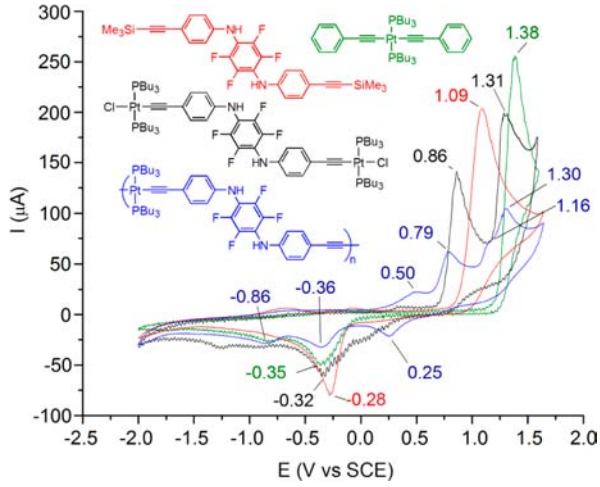

Figure 7. Comparison of the cyclic voltammograms of **4b**, **8b**, **9b**, and [Pt] in absence of acid. All measurements were recorded against a saturated calomel electrode (SCE) with 0.1 M of $TBAPF_6$ supporting electrolyte in DMF. The concentration of the electroactive compounds was 4 mM. The scan rate is 100 mV/s.

using the spacer **4b** (red trace), the *trans*-$C_6H_5C{\equiv}C{-}Pt(PBu_3)_2{-}C{\equiv}CC_6H_5$ ([**Pt**]; green trace), and the model compound **9b**. The model compound exhibits two oxidation waves at 0.86 and 1.31 V vs SCE, which correspond to the oxidation of the diamine residue and the platinum(II) center, respectively, based on the comparison with the traces of **4b** (1.09) and [**Pt**] (1.38 V vs SCE). In the polymers, many waves are observed. The peak at 1.30 V is most likely associated with the platinum(II) center, but the remaining peaks are still in need of in depth analysis.

Molecular Orbital Analysis for the Electrochemical Behavior of the Polymers. The optimized geometry for all the spacers (**4a**, **4b**, **4c**, **5a**, **5b**, and **5c**) and of six model compounds composed of a central *trans*-Pt unit and two diimine or diamine spacers where X = H, F, Cl, were computed for analysis purposes of the electrochemical findings as well as the absorption properties below. The bulk of the MO representations of the frontier orbitals are placed in the Supporting Information and only representative examples are described here.

The CVs indicate that the diamine and diimine species are respectively oxidizable and reducible. The calculated HOMO and LUMO representations exhibit the presence of π and π^* systems (see **5a** and **4a**; Figure 8). For the diimine spacers, the π system is composed of p_z atomic orbital contributions distributed almost evenly on all the C- and N-atoms, consistent with a conjugated unit. The calculated atomic orbital contributions for the LUMO are larger for the quinone diimine center than the rest of the spacer meaning that the reduction

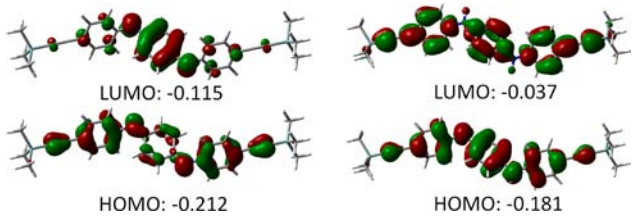

Figure 8. HOMO and LUMO representations for **5a** (left) and **4a** (right).

potentials should be X-dependent. Indeed, this is experimentally observed. The HOMO and LUMO of the diamine species also exhibit evenly distributed p_z orbital atomic contributions, except that some C-atoms show no contribution at all (nodes). This is consistent with the presence of a nonconjugated unit. The HOMO exhibit atomic orbital contributions on the central benzene ring; therefore, the oxidation potential should also be X-dependent. The LUMO is localized at a rather high energy, and consequently the reduction potential of the spacers must be placed at high potentials. Thus, as predicted, the CVs show no wave in the 0 to −2.0 V vs SCE.

The monitoring of the calculated HOMO and LUMO energy levels (Figure 9) indicates that **5c** (X = Cl) is predicted

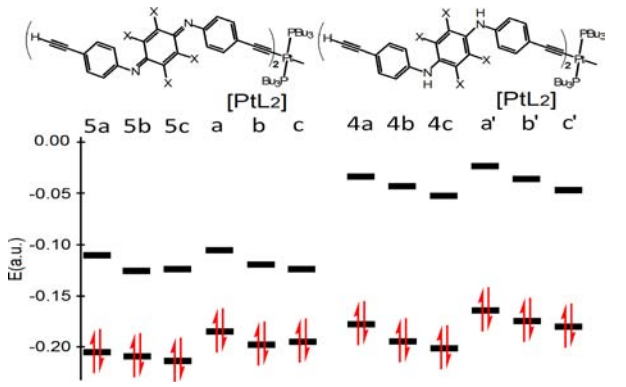

Figure 9. Energy levels for the spacers **4a**, **4b**, **4c**, **5a**, **5b**, and **5c** and of the PtL_2 models X = H ([PtL_2]**a** and ([PtL_2]**a**′), F ([PtL_2]**b** and [PtL_2]**b**′), and Cl ([PtL_2]**c** and ([PtL_2]**c**′).

to be slightly easier to reduce than **5b** (X = F), which are both easier than for **5a** (X = H). Experimentally, this trend is indeed observed (see the return anodic sweeps in Figure 6). Similarly, the oxidation of the diamine spacers is predicted to vary as **4c** (X = Cl) > **4b** (X = F) > **4a** (X = H). This is also noted in the CVs (Figure 5 top).

Using model compounds composed of a central *trans*-Pt unit and two diimine or diamine spacers as side arms denoted as PtL_2 with X = H ([PtL_2]**a**), F ([PtL_2]**b**), Cl ([PtL_2]**c**) for the corresponding polymers, DFT computations generally place both the HOMO and LUMO in a decreasing order going from H to F to Cl, meaning that the reduction potentials, E(red), for the diimine species should vary as E(red) H > F > Cl, and the oxidation potentials, E(oxi), for the diamine species should vary as E(oxi) H < F < Cl.

The HOMO-1, HOMO, LUMO, and LUMO+1 for an optimized geometry of PtL_2 (i.e., [PtL_2]**a**; X = H) as a representative example is provided in Figure 10 (see Supporting Information for the cases where X = F, Cl). The HOMO and HOMO-1 of the diimine-containing species exhibit a π-system, again composed of p_z atomic orbital

dx.doi.org/10.1021/ic300775n | *Inorg. Chem.* 2012, 51, 13081−13095

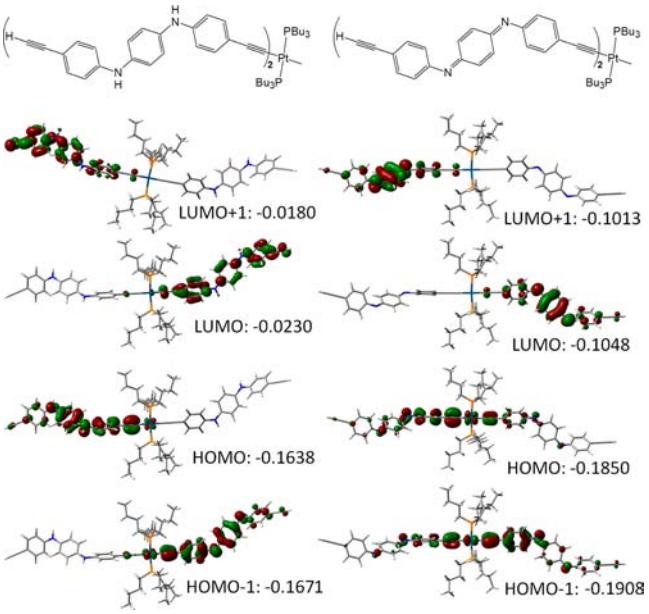

Figure 10. MO representations of the HOMO-1, HOMO, LUMO, and LUMO+1 of optimized geometry of model compounds composed of a $\mathbf{PtL_2}$ (i.e., a Pt unit and two diimine (right) or diamine (left) spacers; X = H ([$\mathbf{PtL_2}$]**a** and [$\mathbf{PtL_2}$]**a**′). The units are in a.u.

contributions, well spreading over the $C_6H_4C{\equiv}CPtL_2C{\equiv}CC_6H_4$ unit with some contributions calculated for atoms of the quinone diimine residues. These two MOs exhibit similar atomic contributions except that the d-orbital used by the Pt metal for conjugation purposes is different (d_{xz} vs d_{yz}). This is due to an attempt to accommodate the relative orientation of the π-systems on both sides of the metal atom. Consequently, the MO energies are bound to be different, and full delocalization of the π-system along the oligomer chain is difficult. The p_z atomic orbital contributions of the LUMO and LUMO+1 of the diimine species are again confined within either one of the π-systems of the quinone diimine fragments. These MOs are clearly not conjugated. The promotion of an electron into these empty π^* MOs would lead to a localized excited state, and the HOMO−LUMO transition would generate a CT excited state involving the Pt atom in the π-systems (HOMO and HOMO-1). So a better description of the lowest energy transition would be CT of the type $C_6H_4CCPtL_2CCC_6H_4$ unit to the central $N{=}C_6X_4{=}N$ unit, mixed with MLCT (metal-to-ligand-charge-transfer).

For the diamine-containing species, the description provided above remains applicable except that some atomic contributions of the Pt atom are also computed for the HOMO and HOMO-1. Consequently, the oxidation potentials are predicted to be bound to be affected by the presence of this atom, as illustrated in Figure 7. The high energy LUMO and LUMO+1 are reminiscent to that of the spacer where practically no Pt-contribution is computed. No reduction wave has been detected in the 0 to −2.0 V vs SCE as well for their corresponding polymers and model compounds.

The diimine-containing materials are colored whereas the diamine analogues are not. These red-shifted bands are due to a CT process from the $-C_6H_4C{\equiv}C-$ unit to the central quinone diimine residue in the spacers and from $Pt(C_6H_4C{\equiv}C)_2$- to the same central component in the model compounds and polymers.[7] This is corroborated by TDDFT, and representative examples are presented for spacers **4b** and **5b** in Table 5 (see the Supporting Information for the others). By assigning a thickness to each bar (in a linear scale of energy), a spectrum that contains no vibronic contribution is computed (Figure 11).

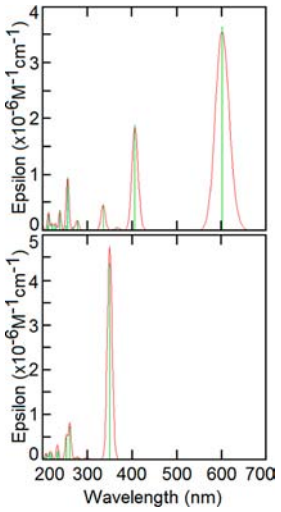

Figure 11. Comparison of the computed UV−vis spectra (excluding vibronic contributions; green bars) by TDDFT for spacers **5b** (up) and **4b** (bottom). The red traces are these same transitions assigned with a 500 cm^{-1} thickness.

Table 5. Computed Singlet−Singlet Transition Energy, Predicted Band Positions, Oscillator Strength (f), and Major Contributions for the First Five Electronic Transitions for Spacers 5b (top) and 4b (bottom)

No.	ν(cm^{-1})	λ(nm)	f	major contributions (%)
			Spacer **5b**	
1	16628	601	1.635	HOMO→LUMO (93)
2	19507	512	0.000	H-1→LUMO (87)
3	24634	405	0.849	H-9→LUMO (24), H-2→LUMO (64)
4	25370	394	0.000	H-3→LUMO (97)
5	26293	380	0.000	H-8→LUMO (27), H-4→LUMO (47), H-1→LUMO (10)
			Spacer **4b**	
1	28579	350	2.182	HOMO→LUMO (98)
2	33504	298	0.014	HOMO→L+2 (92)
3	33798	295	0.000	H-1→LUMO (23), HOMO→L+1 (76)
4	34904	286	0.000	H-1→LUMO (75), HOMO→L+1 (22)
5	36107	276	0.000	HOMO→L+3 (86)

dx.doi.org/10.1021/ic300775n | *Inorg. Chem.* 2012, 51, 13081−13095

The presence of the calculated low-energy absorption characteristics (by TDDFT) presented below corroborate the CT character of this band in these new diimine-containing polymers.

UV−vis Spectroscopy. Typical spectra are presented in Figures 12 and 13 and stress the difference in the spectral finger

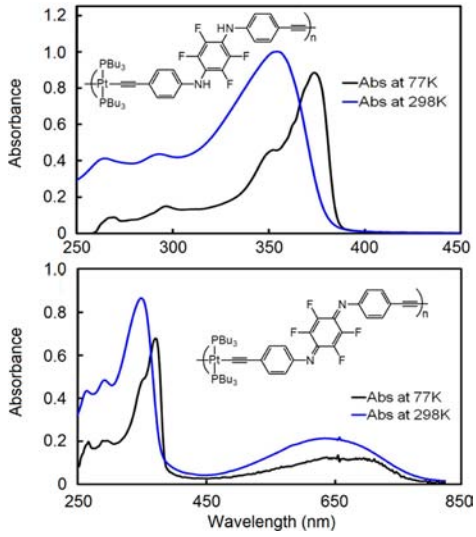

Figure 12. Comparison of the absorption spectra for polymers **8b** and **10b** in 2MeTHF at 298 and 77 K.

prints between the diimine and diamine species. The bulk of the data are placed in Table 6, and the spectra are placed in the Supporting Information.

From the experimental absorption spectral data (Table 6) a clear dependence between the nature of the substituent and the degree of red-shifting is noted for both the diimine and diamine species. This same behavior is also noted in the calculations (Table 7). The comparison between the calculated and experimental data is reasonable for most cases of the diimine and diamine species for the purpose of this work.

The observed temperature-dependence of the absorption spectra illustrated in Figure 12 (and in the Supporting Information, Figures S1−S3) is due to the presence of hot bands at 298 K that disappears at low temperatures. Indeed upon cooling here at 77 K, the vibrational level v = 0 is heavily populated and most, if not all, electronic transitions stem from this level. This explains the sharpening of the low-energy part of the absorption. Moreover, the presence of single bonds in the molecular structures makes the conformation variable in fluid solution at the moment of the absorption for samples at 298 K. This would contribute at making the absorption band larger. Upon cooling to 77 K, the rigidity of the medium and the decrease of thermal energy prevent or minimize such degree of freedom, hence also rendering the absorption band sharper.

For the diimine-containing materials the comparison is not as good as at first glance. This is because the experimental value is taken at the maximum of the low energy band since the position of the pure electronic transition is not perceptible at this temperature. Upon cooling, several materials exhibit some vibronic structures denoted as broad components. For example, polymer **10b** (bottom of Figure 12) exhibits a first feature at ~700 nm (experimental), which compares favorably with the computed singlet−singlet transitions of 685 nm (for [$\mathbf{PtL_2}$]**b**). Conversely, the comparison is more difficult as discrepancies of

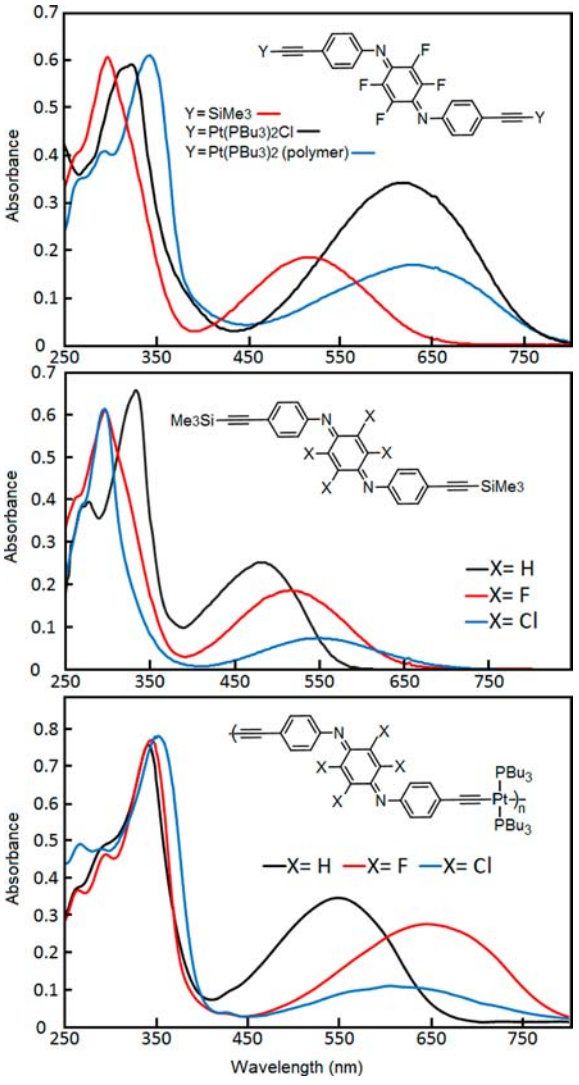

Figure 13. Comparison of **5b**, **10b**, and **11b** (top), of **5a**, **5b**, and **5c** (middle), and of **10a**, **10b**, and **10c** in CH_2Cl_2 at 298 K. Because the absorptivity varies from material to material because of the mixed-valence nature for some of these, and the fact that these are polymers that exhibit a molecular weight distribution, it is difficult to put the spectra on a discrete extinction coefficient scale. Consequently, the absorbance was normalized on the 300−350 nm peak.

146 and 148 nm are found between the calculated and the experimental values for **5c** and **10c**, respectively. This is due to the fact that these transitions are calculated using the ground state conformation and does not take into account the possibly large excited state distortions. Nevertheless, the lowest energy CT bands of the oxidized species are rightfully calculated to be red-shifted with respect to those of the reduced species. As a whole, the TDDFT calculations corroborate the CT nature of the lowest excited state and the X-dependence of the electronic spectra.

Transient Absorption. The ns transient absorption spectra were studied to address the behavior in the triplet state with regards to electron transfer. It is known that aromatic amines transfer electron to imines under flash irradiation.[17] Relevant for this work, the T_1-T_n transient absorption spectra of *N*,*N*′-diphenyl-1,4-diaminobenzene is characterized by two strong transient absorptions at 400 (narrow) and 700 nm (very broad) at −130 °C.[17c] The transient spectrum of the related derivative

dx.doi.org/10.1021/ic300775n | *Inorg. Chem.* 2012, 51, 13081−13095

Table 6. UV-vis Data in 2MeTHF at 298 K

materials	λ(nm) (ε(M^{-1} cm^{-1}))			
4a		300 (34600)	340 (60300)	
4b			323 (61900)	
4c		275 (38900)	325 (29600)	
5a		274 (26100)	305 (31900)	470 (10700)
5b		260 (28000)	295 (48900)	515 (13700)
5c		261 (67900)	300 (90900)	520 (18600)
9a	*a*			
9b	244 (53000)		340 (101400)	
9c	242 (42500)	270 (35350)	336 (47800)	
11a	241 (31700)		324 (48800)	533 (22100)
11b	*b*			
11c	243 (25500),		330 (25500)	605 (9950)
8a	*a*			
8b	260 (49000)	290 (28000)	350 (70200)	
8c		274 (37500)	360 (37500)	
10a		290 (45800)	335 (46900)	545 (20100)
10b	247 (22200)	265 (22200)	350 (22200)	630 (5640)[c]
10c		268 (42550)	350 (58800)	610 (7570)[c]

[a]Polymer not available. [b]Not measured. [c]Mixed-valence.

Table 7. Comparison of the Computed Singlet−Singlet Transitions of the Spacers and Models Composed of PtL_2[a] in Their Ground State Optimized Geometry[b] with the Experimental Values (in 2MeTHF) at 77 K (in Parentheses)

	diimines			diamines	
compounds	ν (cm^{-1})	λ (nm) (λ_{exp})[c]	compounds	ν (cm^{-1})	λ (nm) (λ_{exp})[c]
5a	17686	565 (~480)	**4a**	27750	362 (~358)
5b	17779	601 (~525)	**4b**	27127	350 (~335)
5c	17335	728 (~485)	**4c**	25696	353 (~345)
[PtL_2]**a**	15481	646 (~600)	[PtL_2]**a′**	26556	376 (~378)[d]
[PtL_2]**b**	14596	685 (~700)	[PtL_2]**b′**	26983	370 (~370)
[PtL_2]**c**	12073	828 (~680)	[PtL_2]**c′**	24700	404 (~380)

[a]That is, a Pt unit and two diimine or diamine spacers. [b]Using a THF polarizable continuum solvation model. [c]The experimental values (±3 nm) are those for the spacers and polymers. The spectra for the latters exhibit a low-energy shoulder attributable to the 0−0 peak. [d]Polymer not available. Data for complex **9a**.

4a exhibits the same features but shifted to 475 and ~870 nm (top right; Figure 14) at 298 K. The red-shift of the signal can be attributed to the replacement of the H-atoms with −C≡$CSiMe_3$ units by virtue of conjugation. These transient species can safely be assigned to T_1-T_n as well. Upon the replacement of X = H by F (**4b**; Figure 14, middle right), the transient spectra still exhibit the signal at ~400 nm, but the red-shifted transient band has become much weaker at 298 K. Conversely to previous studies on *N*,*N*′-diphenyl-1,4-diaminobenzene,[17c] the decays are biphasic for both **4a** (~25 ns and ~0.1 ms) and **4b** (~90 ns and > several hundred μs, i.e., not precisely evaluated); the traces are placed in the Supporting Information). Because this behavior is observed only for the reduced species, one can suspect that **4a** and **4b** behaves as a dual chromophore as they are not conjugated.

For the *N*,*N*′-diphenylquinone diimine or any of its closely related derivatives, to the best of our knowledge there is no transient absorption spectra reported so far. The transient spectra of **5b** exhibits a well-defined feature to ~450 nm (decaying with a ~26 ns lifetime; Supporting Information) with no strong absorption in the red region of the spectrum (Figure 14, top left), which differs from the corresponding diamine. Upon the replacement of the $SiMe_3$ substituent by $Pt(PBu_3)_2Cl$ (Figure 14, middle left), the general shape of the transient spectra remains similar. Importantly, the signal remains well-defined but the decay shortens to ~6 ns (Supporting Information) meaning that the presence of the heavy Pt-atom modestly enhances the rate of T_1 deactivation by virtue of spin−orbit coupling and intersystem crossing (the decrease is only from 26 to 6 ns).

Relevant to design of mixed valence organometallic versions of PANI for X = F (**10b**), it was important to monitor the transient signal of the totally reduced polymer for this same substituent (X = F, **8b**). Experimentally, both transient spectra are weak and very similar (Figure 14, bottom). Notably, the well-defined feature of the characteristic of the diimine species is totally absent meaning that its triplet excited state is quenched. On the basis of earlier works mentioned above,[17] one can speculate that a photoinduced electron transfer occurs from the rich diamine unit to the poorer diimine fragment of the backbone of polymer **10b**. Because the signals were generally weak, it was not possible to perform kinetic analysis on our instrument (i.e., no decay traces was observed; Supporting Information), but the main observation of these measurements is that the efficient quenching takes place when the diamine unit is substituted with F (and Cl since there was no signal as well), and that the coupling of the diamine unit with the diimine leads to quenching of the T_1 species of the diimine residues.

dx.doi.org/10.1021/ic300775n | *Inorg. Chem.* 2012, 51, 13081−13095

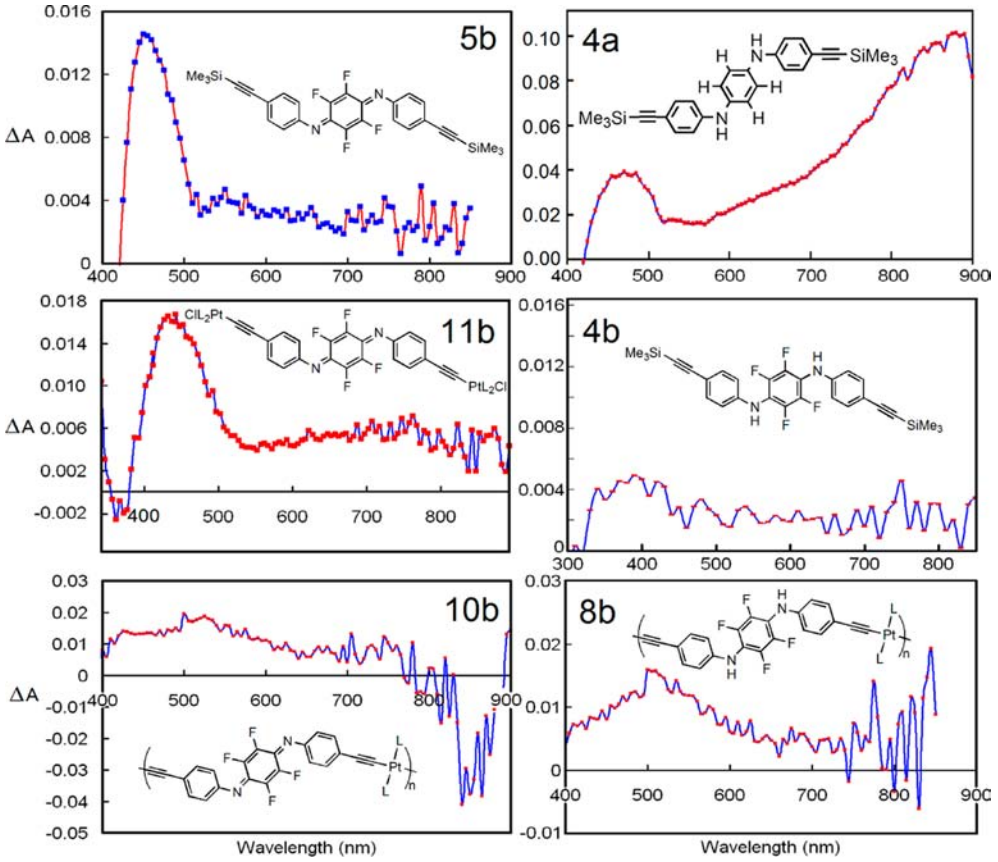

Figure 14. Comparison of the transient absorption spectra of **4a**, **4b**, **5b**, **8b**, **10b**, and **11b** at 298 K in degassed 2MeTHF. λ_{exc} = 355 nm and no delay time between the pump and probe pulses was applied. This delay time was selected because the signals are generally weak. Please note that **10b** is in mixed-valence form.

Table 8. Comparison of the Polymer Properties for Various Substituents

	X				
	CH_3	H	OMe	F	Cl
nature of the polymer	oxidized	oxidized	oxidized and mixed	mixed and reduced	mixed and reduced
length of the polymer (GPC)	19 units	26 units	38 units	14 units	10 units
thermal stability (TGA; °C)	>280	>250	>300	>350	
electrochemical response in DMF + 2.7 M TFA (all chemically rev.)	1 quasi-rev. wav.	2 quasi-rev. wav.		2 quasi-rev. wav.	2 quasi-rev. wav.
potential of the center of the wave (in DMF + 2.7 M TFA V vs SCE)	~ +0.46	~ +0.40		~ +0.45	~ +0.45
		~ +0.60		~ +0.65	~ +0.65
position of the CT band (nm)	502	545	560	630	610
absorptivity (CT band in M^{-1} cm^{-1})	23400	20100	13700	5640[a]	7570[a]
average dihedral angle benzoquinone-phenyl (deg)	49.3	56.2	69.4	52.2	75.2

[a]Exist as mixed-valence form, so the absorptivity may be under evaluated.

CONCLUDING REMARKS

Attempts to obtain all organometallic versions of PANI were made taking advantage of the beneficial effect of substitution. Hence, this work aimed at defining what controls the electronic properties of these polymers. Comparison with previous works (Table 8) indicates trends. Electron withdrawing substituents tend to stabilize the reduced form whereas the electron donating groups tend to provide the oxidized form only. These substituents appear to be acting as moderators ensuring that the benzoquinone is not too electron poor and the 1,4-diaminobenzene is not too electron rich. The mixed-valence form was successfully prepared for X = OMe, F, and Cl, where the method to obtain them differs for OMe (from a mixture of benzoquinone and 1,4-diaminobenzene precursors) from F and Cl (from the benzoquinone precursor).

In all cases, the polymers have been prepared as oligomers where the longest one is for X = OMe. It is not yet clear whether the solubility plays a role on this property, it appears possible to vary the chain length on the benzoquinone using OEt for example.[7] The thermal stability also shows a rough relationship between electron donating (lesser stable) and withdrawing substituents (more stable). Four of these systems were studied in acid solutions and exhibited one or two chemically or quasi-chemically reversible waves in DMF. In

dx.doi.org/10.1021/ic300775n | Inorg. Chem. 2012, 51, 13081−13095

other words, under these conditions the polymers exist as the organometallic version of PANI in its protonated emaraldine forms. The electrochemical waves are large, and all appear in the same potential window (~+0.40 to +0.45 and ~+0.60 to 0.65 V vs SCE). The electron donating and withdrawing properties of the substituents were clearly demonstrated by UV−vis spectroscopy by monitoring the position of the CT band in the oxidized materials. This band which gives rise to the highly colored materials is more red-shifted as the electron withdrawing behavior of the substituent increases. The absorptivity properties are approximately the same for X= CH_3 and H, but decrease going to F and Cl. The reason for this is that to obtain the oxidized version, the polymer must accommodate the presence of some reduced units in the chain. So the ε values are bound to be lower than expected. The ratio deduced from ^{1}H NMR (from the NH signal) is approximately 1/3 oxidized vs reduced. By multiplying the reported ε values by 3, then the extrapolated values would fall in the correct range observed for the pure oxidized materials. These observations suggest that the reduced and oxidized units along the same polymer chain must interact together to explain their stability and coexistence. Indeed, evidence of such interactions was corroborated by monitoring the triplet transient species and total quenching of the T_1-T_n absorption was observed in the mixed-valence polymers. In our previous studies we reported that the oxidized species do not exhibit luminescence from the lower CT excited state. We come to the conclusion that this behavior must be general. The investigation of a large number of X-ray structures of spacers and model compounds showed that the dihedral angle between the average benzoquinone plane and that of the flanking phenyls vary a lot. Some correlation between the size of the substituent and the C═N bond length has been noted, therefore monitoring the relative degree of conjugation, but the same exercise on the corresponding 1,4-diaminobenzene, a non-conjugated system, shows that there is still some notable variation of C−N bond length.We have now succeeded at preparing or generating all four forms of PANI in its organometallic version (with *trans*-C≡CPtL$_2$C≡C; L = monophosphine). The totally reduced form was the missing component. We also consider this work a useful data bank for the design of benzoquinone diimine-based materials, which also are important for the design of very low band gap polymers. Future work will indeed report the design of such polymers where the electron donor and acceptor moieties in the backbone of the polymer can be changed to form highly absorbing (ε values in the 10^5 M^{-1} cm^{-1} range) materials exhibiting highly red-shifted CT bands (reaching 900 nm). Indeed, preliminary results for examples of such low band gap polymers based on benzoquinone diimines were just published by us.[18]

■ ASSOCIATED CONTENT

Supporting Information

X-ray crystallographic data in CIF format, experimental section, crystal data, absorption spectra at 298 and 77 K, frontier MO representations (DFT), calculated pure electronic transitions and calculated spectra (TDDFT), CV traces of the compounds and polymers in the presence and absence of acid and transient decay curves. This material is available free of charge via the Internet at http://pubs.acs.org.

■ AUTHOR INFORMATION

Corresponding Author

*E-mail: Pierre.Harvey@USherbrooke. Fax: 819-821-8017. Phone: 819-821-7092.

Notes

The authors declare no competing financial interest.

†On leave from the Chemistry Department, Faculty of Sciences, Assiut University, Assiut, Egypt.

■ ACKNOWLEDGMENTS

This research was supported by the Natural Sciences and Engineering Research Council of Canada (NSERC), le Fonds Québécois de la Recherche sur la Nature et les Technologies (FQRNT), the Centre Québécois des Matériaux Fonctionnels (CQMF), and the Centre d'Études des Matériaux Optiques et Photoniques de l'Université de Sherbrooke (CEMOPUS).

■ REFERENCES

(1) Pound, J. R. *J. Phys. Colloid Chem.* **1947**, *51*, 378−82.

(2) (a) Kane-Maguire, L. A. P.; Wallace; Gordon, G. *Chem. Soc. Rev.* **2010**, *39*, 2545−2576. (b) Fang, F. F.; Lee, B. M.; Choi, H. J. *Macromol. Res.* **2010**, *18*, 99−112. (c) Rohwerder, M. *Int. J. Mater. Res.* **2009**, *100*, 1331−1342. (d) Guiseppi-Elie, A. *Biomaterials* **2010**, *31*, 2701−2716. (e) Ates, M.; Sarac, A. S. *Prog. Org. Coat.* **2009**, *66*, 337−358. (f) Li, D.; Huang, J.; Kaner, R. B. *Acc. Chem. Res.* **2009**, *42*, 135−145. (g) Zeysing, B.; Wessling, B. B.; Christoph, J.; Dyakonov, V.; Scherf, U. *Org. Photovoltaics* **2008**, 243−260. (h) Reda, M. *Mater. Perform.* **2007**, *46*, 40−42. (i) Kane-Maguire, L. A. P.; Wallace, G. G. *Polym. News* **2000**, *25*, 293−298. (j) Alonso, J. L.; Ferrer, J. C.; De Avila, S.; Fernandez. *J. Optoelectron. Adv. Mater.* **2008**, *10*, 3150−3157. (k) Yin, Z.; Zheng, Q. *Adv. Energy Mater.* **2012**, *2*, 179−218. (l) Ibrahim, M.; Bassil, M.; Demirci, U. B.; Khoury, T.; El Haj Moussa, G.; El Tahchi, M.; Miele, P. *Mater. Chem. Phys.* **2012**, *133*, 1040−1049. (m) Wang, G.; Xing, W.; Zhuo, S. *Electrochim. Acta* **2012**, *66*, 151−157. (n) Peng, S.; Liang, J.; Mhaisalkar, S. G.; Ramakrishna, S. *J. Mater. Chem.* **2012**, *22*, 5308−5311. (o) Lim, T. H.; Oh, K. W.; Kim, S. H. *Synth. Met.* **2012**, *162*, 268−275. (p) Tang, Z.; Wu, J.; Liu, Q.; Zheng, M.; Tang, Q.; Lan, Z.; Lin, J. *J. Power Sources* **2012**, *203*, 282−287. (q) Peng, S.; Zhu, P.; Wu, Y.; Mhaisalkar, S. G.; Ramakrishna, S. *RSC Adv.* **2012**, *2*, 652−657. (r) Wang, G.; Zhuo, S.; Xing, W. *Mater. Lett.* **2012**, *69*, 27−29. (s) Joshi, R. A.; Taur; Vidya, S.; Sharma, R. *Sol. Energy* **2012**, *86*, 301−306. (t) Chamier, J.; Crouch, A. M. *Mater. Chem. Phys.* **2012**, *132*, 10−16. (u) Ebrahim, S. *Polym. Sci., A* **2011**, *53*, 1217−1226. (v) Bourdo, S. E.; Saini, V.; Piron, J.; Al-Brahim, I.; Boyer, C.; Rioux, J.; Bairi, V.; Biris, A. S.; Viswanathan, T. *ACS Appl. Mater. Interfaces* **2012**, *4*, 363−368. (w) Joshi, R. A.; Taur, V. S.; Sharma, R. *J. Non-Cryst. Solids* **2012**, *358*, 188−195. (x) Ajit, S.; Palaniappan, S.; Kumar, P. U.; Madhusudhanachary, P. *J. Polym. Sci., A: Polym. Chem.* **2012**, *50*, 884−889.

(3) (a) Huang, K.-Y.; Jhuo, Y.-S.; Wua, P.-S.; Lin, C.-H.; Yu, Y.-H.; Yeh, J.-M. *Eur. Polym. J.* **2009**, *45*, 485−493. (b) Breza, M.; Kortisova, I.; Cibulkova, Z. *Polym. Degrad. Stab.* **2006**, *91*, 2848−2852. (c) Marczewska, B.; Przegalinski, M.; Wiadomosci. *Chemiczne* **2009**, *63*, 1115−1143.

(4) (a) Morishita, H.; Kawamura, H.; Hosokawa, C. *PCT Int. Appl.* WO 2007116750 A1 20071018, 2007. (b) Nakaie, N.; Yamada, T. *PCT Int. Appl.* WO 2010041701 A1 20100415, 2010.

(5) Hiroshi, W. A.; Dominique de Caro, L. V.; Tatsuhiko, O.; Yoshimasa, B.; Takehiko, M. *Thin Solid Films* **2009**, *518*, 299−304.

(6) Gadomsky, S. Y.; Varlamov, V. T. *Russ. Chem. Bull., Int. Ed.* **2007**, *56*, 2376−2383.

(7) (a) Gagnon, K.; Aly, S. M.; Fortin, D.; Abd-El-Aziz, A. S.; Harvey, P. D. *J. Inorg. Organomet. Polym. Mater.* **2009**, *19*, 28−34. (b) Fortin, D.; Clément, S.; Gagnon, K.; Bérubé, J.-F.; Harvey, P. D. *Inorg. Chem.* **2009**, *48*, 446−454. (c) Gagnon, K.; Bérubé, J.-F.; Bellows, D.; Caron, L.; Aly, S. M.; Wittmeyer, A.; Alaa Abd-El-Aziz, A. S.; Fortin, D.; Harvey, P. D. *Organometallics* **2008**, *27*, 2201−2214.

(8) Ueda, F.; Mukai, K.; Harada, I.; Nakajima, T.; Kawagoe, T. *Macromolecules* **1990**, *23*, 4925−4928.
(9) (a) de Santana, H.; Quillard, S.; Fayad, E.; Louarn, G. *Synth. Met.* **2006**, *156*, 81−85. (b) Han, C.-C.; Balakumar, R.; Thirumalai, D.; Chung, M.-T. *Org. Biomol. Chem.* **2006**, *4*, 3511−3516. (c) Nishiumi, T.; Chimoto, Y.; Hagiwara, Y.; Higuchi, M.; Yamamoto, K. *Macromolecules* **2004**, *37*, 2661−2664.
(10) (a) Nishiumi, T.; Nomura, Y.; Chimoto, Y.; Higuchi, M.; Yamamoto, K. *J. Phys. Chem. B* **2004**, *108*, 7992−8000. (b) Temme, O.; Laschat, S.; Frohlich, R.; Wibbeling, B.; Heinze, J.; Hauser, P. *J. Chem. Soc., Perkin Trans. 2* **1997**, 2083−2085.
(11) Turovska, B.; Stradins, J.; Glezer, V.; Lokmane, E.; Sarule, E.; Freimanis, J. *Z. Akad. Vestis, Kimi. Serija* **1989**, 108−15.
(12) Garcia-Canadas, J.; Lafuente, A.; Rodriguez, G.; Marcos, M. L.; Gonzalez Velasco, J. *J. Electroanal. Chem.* **2004**, *565*, 57−64.
(13) Kershman, J. R.; Paris, K. E.; Stamey, J. A.; Pyati, R. *J. Electroanal. Chem.* **2006**, *597*, 87−94.
(14) Kondrachova, L.; Paris, K. E.; Sanchez, P. C.; Vega, A. M.; Pyati, R.; Rithner, C. D. *J. Electroanal. Chem.* **2005**, *756*, 287−294.
(15) Varlamov, V. T. *Mendeleev Commun.* **2003**, *13*, 33−34.
(16) Moriuchi, T.; Bandoh, S.; Miyaishi, M.; Hirao, T. *Eur. J. Inorg. Chem.* **2001**, 651−657.
(17) (a) Fitzgerald, E. A., Jr.; Wuelfing, P., Jr.; Richtol, H. H. *J. Phys. Chem.* **1971**, *76*, 2737−2741. (b) Bensasson, R. *J. Phys. Chem.* **1968**, *78*, 3774−3782. (c) Linschitz, H.; Ottolenghi, M.; Bensasson, R. *J. Am. Chem. Soc.* **1967**, *89*, 4592−4599.
(18) Lamare, S.; Aly, S. M.; Fortin, D.; Harvey, P. D. *Chem.Commun.* **2011**, *47*, 10942−10944.